Journal of Alloys and Compounds 518 (2012) 44–50

Contents lists available at SciVerse ScienceDirect

Journal of Alloys and Compounds

journal homepage: www.elsevier.com/locate/jallcom

Microstructure and dielectric properties of highly tunable $Ba_{0.6}Sr_{0.4}TiO_3/MgO/Al_2O_3/ZnO$ composite

Guoxin Hu, Feng Gao*, Liangliang Liu, Bei Xu, Zhengtang Liu

State Key Laboratory of Solidification Processing, Northwestern Polytechnical University, Xi'an Shaanxi 710072, PR China

ARTICLE INFO

Article history:
Received 5 July 2011
Received in revised form
19 December 2011
Accepted 21 December 2011
Available online 29 December 2011

Keywords:
Barium strontium titanate
Dielectric properties
Paraelectric–ferroelectric
Tunability

ABSTRACT

The effect of co-doping ZnO, Al_2O_3 and MgO on the microstructures and dielectric properties of $Ba_{0.6}Sr_{0.4}TiO_3$ ceramics prepared by the mixed-oxide route at 1400 °C was investigated. And a comparison criterion for the BST-based tunable ceramics was proposed. The results show that a cubic perovskite phase $Ba_{0.6}Sr_{0.4}TiO_3$ and a face-centered-cubic spinel phase $Mg(Zn)Al_2O_4$ were observed in $BST/MgO/Al_2O_3/ZnO$ (BMAZ) composite ceramics. When Zn^{2+} content exceeds solid solubility limit in the BST, excess ZnO will react with Al_2O_3 to produce $ZnAl_2O_4$ phase. With the increase of ZnO, the paraelectric–ferroelectric phase transition points of BMAZ ceramics shift to the lower temperatures, and the maximum of dielectric constant increased first and then decreased. A higher tunability which amounts to 27.4% under 1.0 kV/mm biasing was obtained for BMAZ ceramics doped with 1.0 wt% ZnO.

1. Introduction

Barium strontium titanate (BST), which is a solid solution of barium titanate ($BaTiO_3$) and strontium titanate ($SrTiO_3$), is a well-known ceramic capacitor dielectric material in electronic industry. It has the merit of high dielectric non-linearity (a large dielectric constant change under dc bias electric field) and low dielectric loss above the ferroelectric Curie temperature [1–4], which renders it to be one of the most promising materials to realize the application of tunable ceramic capacitors, dielectric filters, phase shifters and other tunable microwave devices [5–7]. However, pure BST ferroelectric ceramics is not suitable for such applications due to its high dielectric constant at room temperature and thus difficult to satisfy the requirement of impedance matching and high power in microwave device designs [8]. Hence it is desirable to lower the dielectric constant without deteriorating the tunability and dielectric loss.

Ferroelectric and dielectric properties of BST ceramics strongly depend on the sintering conditions, grain size, porosity, doping amount and structural defects [9–11]. These parameters as well as dielectric properties may also be modified by the substitution of selected elements for A or B site atoms of the ABO_3 perovskite structure [12]. The strong influence of the heterovalent B site dopants such as Mg^{2+}, Al^{3+} on the grain structure and electric properties of $Ba_{0.6}Sr_{0.4}TiO_3$ ceramics was reported [13]. It is reported that the piezoelectric properties of the $Bi_{0.5}Na_{0.5}TiO_3$ ceramics was improved by doping with 0.5 wt% ZnO [14]. ZnO has been previously used on KNN in an attempt to reduce the dielectric losses of the material. It has been shown that addition of ZnO helps to increase the density of the material and avoids the deliquescence [15]. For $Ba_{0.3}Sr_{0.7}TiO_3$ ceramics, doping with 1.6 wt% ZnO will improve dielectric properties and breakdown strength [16].

In order to further investigate the effect of ZnO doping on the microstructure and dielectric properties of $Ba_{0.6}Sr_{0.4}TiO_3/MgO/Al_2O_3$ composite ceramics, the dielectric tunable properties of $Ba_{0.6}Sr_{0.4}TiO_3/MgO/Al_2O_3/ZnO$ (BMAZ) have been measured under the applied bias. The higher tunability of BMAZ ceramics was obtained for the development of practically tunable components.

2. Experimental procedures

The conventional ceramic processing method was employed to prepare $Ba_{0.6}Sr_{0.4}TiO_3/MgO/Al_2O_3/ZnO$ ceramic samples. $Ba_{0.6}Sr_{0.4}TiO_3$ powders were first prepared by the conventional solid-state reaction method: the starting raw materials, $BaCO_3$ (99.88%), $SrCO_3$ (99.0%) and TiO_2 (98.0%) powders, were weighed according to the stoichiometry. The raw materials were then mixed together using alcohol and zirconia milling media for 12 h. After drying, the mixture was calcined at 1050 °C for 2 h in air. Then 10 wt% MgO (98.0%), 20 wt% Al_2O_3 (99.0%) and various amounts of ZnO (99.0%) (x = 0.5, 1.0, 2.0, 4.0, 5.0, 10.0, 15.0, 20.0 wt%) were added into the BST powders (denoted BMAZ1–8#), and ball-milled for 12 h and dried. The obtained powders were pulverized with 5 wt% polyvinyl alcohol (PVA) binder and pressed into disk-shaped pellets under 100 MPa. The green pellets of the composite ceramics were sintered at 1400 °C for 2 h in air. Silver paste was sintered on both sides of the samples at 500 °C for 15 min to form electrodes for the electrical measurements.

* Corresponding author at: School of Material Science and Engineering, Northwestern Polytechnical University, Xi'an 710072, PR China. Tel.: +86 13096956133.
E-mail address: gaofeng@nwpu.edu.cn (F. Gao).

0925-8388/$ – see front matter.
doi:10.1016/j.jallcom.2011.12.105

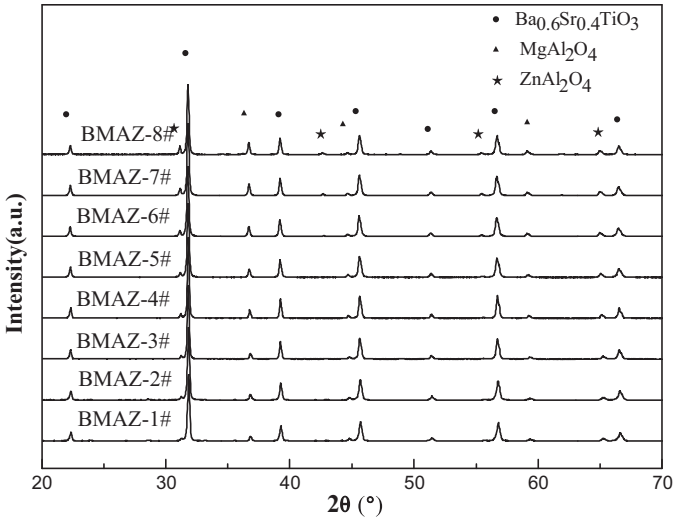

Fig. 1. XRD patterns of BMAZ1–8# ceramics.

X-ray diffraction analysis (XRD, X'pert MPD PRO, Holland) with Cu Kα radiation was used for phase identification. A scanning electron microscope (SEM, Supra 55, Germany) equipped with an energy-dispersive spectrometer (EDS) was used to characterize the microstructure and chemical component elements. The temperature dependence of dielectric constant and loss tangent was measured using a high-precision LCR meter (HP4284A) connected with a temperature controlled chamber. The tunability of the material is determined by the following equation:

$$\text{Tunability}\ \ \% = \frac{\varepsilon(E_0) - \varepsilon(E)}{\varepsilon(E_0)} \times 100 \quad (1)$$

where $\varepsilon(E_0)$ and $\varepsilon(E)$ are the dielectric permittivity under zero dc electric field and under a specific electric field respectively.

3. Results and discussion

Fig. 1 shows the X-ray diffraction pattern of BMAZ composite ceramic samples. The cubic perovskite phase $Ba_{0.6}Sr_{0.4}TiO_3$ and the face-centered-cubic spinel phase $MgAl_2O_4$ and $ZnAl_2O_4$ with no obvious shift of diffraction peaks are observed in all ceramic samples. As the content of ZnO increases, $MgAl_2O_4$ and $ZnAl_2O_4$ peaks are obviously raised, while $Ba_{0.6}Sr_{0.4}TiO_3$ peak is slightly depressed relative to $ZnAl_2O_4$.

To further discuss Zn^{2+} doping mechanism in the BST lattice, the tolerance factor t of different dopants was calculated according to Eq. (2):

$$t = \frac{r_A + r_O}{\sqrt{2}(r_B + r_O)} \quad (2)$$

where r_A and r_B are the ionic radius of the ions occupying the A, B positions, and r_O is the ionic radius of oxygen. It has been observed that a stable perovskite may be expected to form if $t = 0.77–1.09$. The closer the tolerance factor t approaches 1, the more stable the perovskite structure is. Ferroelectric perovskites with $t = 1$ may be expected to have a cubic symmetry, ferroelectric perovskites with $t < 1$ are usually rhombohedral or monoclinic while ferroelectric perovskites with $t > 1$ are commonly tetragonal [17]. The calculated tolerance factor results are list in Table 1. When Zn^{2+}, Mg^{2+}, Al^{3+} occupy B position, the tolerance factors are respectively 0.8796, 0.9182, 0.9908. While these ions occupy A position, the tolerance factors are less than 0.77. It indicates that Zn^{2+} will enter the BST lattice to occupy B position to substitute Ti^{4+}, but the tendency of Zn^{2+} substituting Ti^{4+} is weaker than that of Mg^{2+} and Al^{3+}.

During the sintering process of BMAZ ceramics, Zn^{2+}, Mg^{2+} and Al^{3+} ions act as the acceptor dopants, just as follows:

$$ZnO \xrightarrow{BST} Zn''_{Ti} + V_O^{\bullet\bullet} + O_O \quad (3)$$

Table 1
The tolerance factors of the dopants.

Dopants	Ionic radius/pm	Position	t
Mg^{2+}	65	A	0.6970
		B	0.9182
Al^{3+}	50	A	0.6460
		B	0.9908
Zn^{2+}	74	A	0.7275
		B	0.8796

$$MgO \xrightarrow{BST} Mg''_{Ti} + V_O^{\bullet\bullet} + O_O \quad (4)$$

$$Al_2O_3 \xrightarrow{BST} 2Al'_{Ti} + V_O^{\bullet\bullet} + 3O_O \quad (5)$$

According to MgO–Al_2O_3 and ZnO–Al_2O_3 binary phase diagrams [18,19], MgO reacts with Al_2O_3 to produce $MgAl_2O_4$ spinel phase at ~1000 °C, and ZnO reacts with Al_2O_3 to produce stable $ZnAl_2O_4$ spinel phase below ~1900 °C. When Zn^{2+} content exceeds solid solubility limit in the BST, more $ZnAl_2O_4$ phase will be produced.

Fig. 2 shows the lattice constants of BMAZ ceramics doped with different amounts of ZnO. The value of the lattice constants is calculated by the least square method. The lattice constant of BMAZ firstly increases then decreases gradually. It can be explained that more and more Zn^{2+} with larger ionic radius substitute Ti^{4+} at first, while when Zn^{2+} content exceed solid solubility limit in the BST, excess ZnO (>2 wt%) will react with Al_2O_3 to produce a mass of $ZnAl_2O_4$ spinel phase. Thus more Ba^{2+} and Sr^{2+} with larger ionic radius will enter into $ZnAl_2O_4$ and $MgAl_2O_4$ to substitute Zn^{2+} and Mg^{2+}, resulting in the decrease of the lattice constant of BMAZ. This will be verified by the following SEM analysis.

The SEM images of samples are shown in Fig. 3. It is clear that two component phases co-exist and all the samples are dense and voids-free. There is similar grain morphology in different samples, comprising of dark and light cubic lumpish grains. The energy dispersive spectroscopy (EDS) patterns and data for BMAZ-4# sample are shown in Fig. 4 and Table 2. It can be detected that the dark grains contain primarily Mg, Al, O and small amounts of Ba, Sr, Ti, Zn element. The light grains contain primarily Ba, Sr, Ti, O and small amounts of Mg, Al element. According to the EDS data, it can be concluded that the dark grains and the light grains are (Mg, Zn)Al_2O_4 and $Ba_{0.6}Sr_{0.4}TiO_3$, respectively, moreover, inter-diffusion exists between $Ba_{0.6}Sr_{0.4}TiO_3$ and (Mg, Zn)Al_2O_4. With increasing of ZnO content, two different grains grow larger and larger together. It is concluded that the addition of ZnO will promote the densification and the grain growth of BMAZ ceramics.

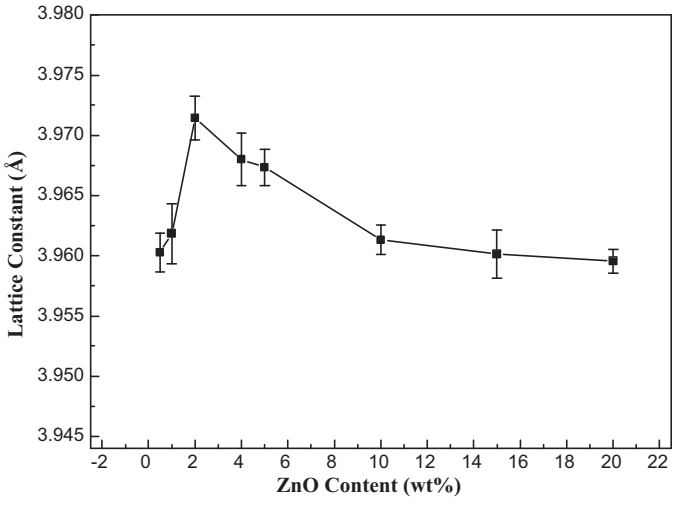

Fig. 2. The lattice constants of BMAZ ceramics doped with different amounts of ZnO.

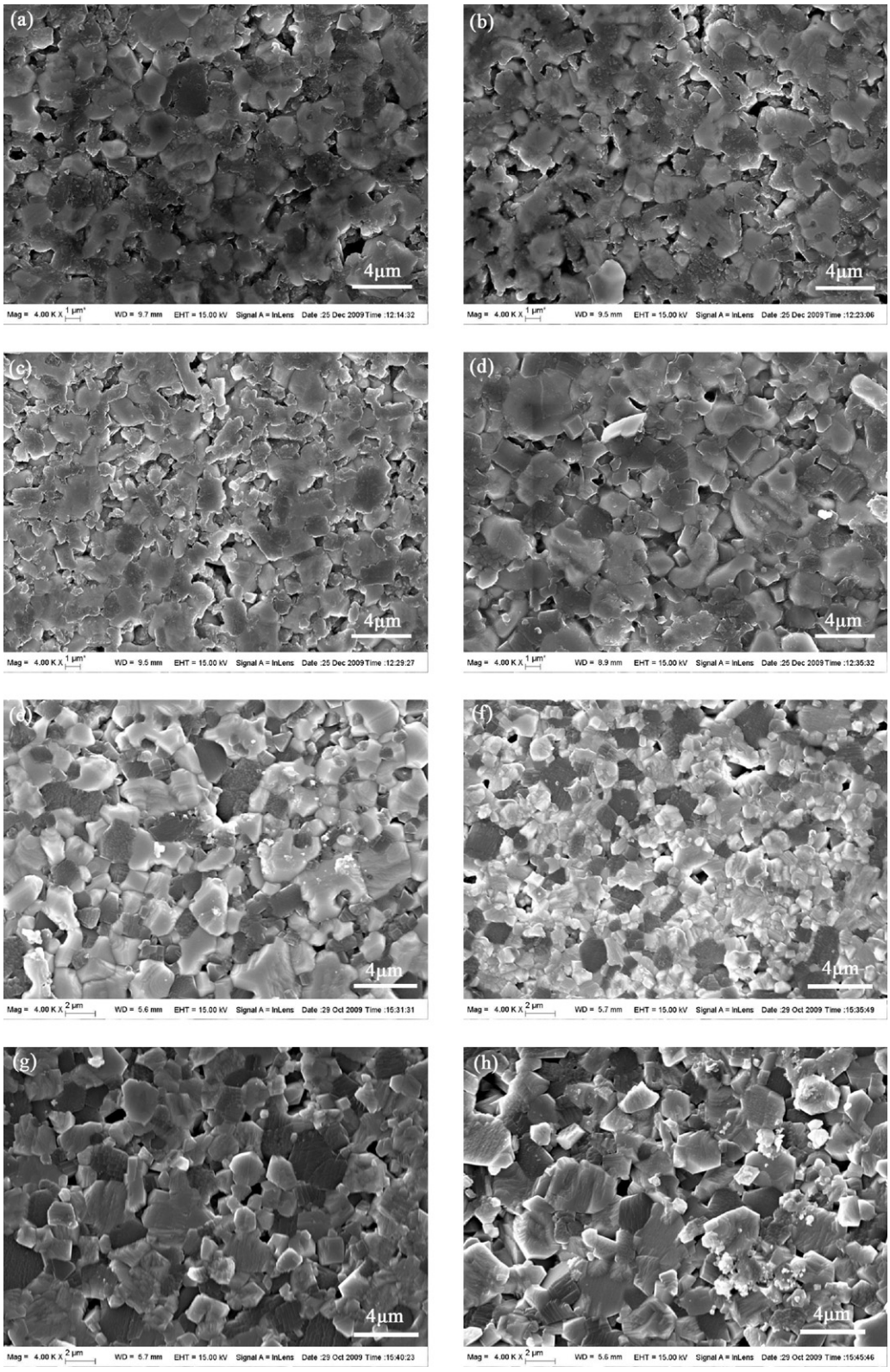

Fig. 3. SEM images of BMAZ ceramics doped with various amounts of ZnO: (a) 0.5 wt%, (b) 1.0 wt%, (c) 2.0 wt%, (d) 4.0 wt%, (e) 5.0 wt%, (f) 10.0 wt%, (g) 15.0 wt%, (h) 20.0 wt%.

Dielectric constant and dielectric loss of BMAZ ceramics are shown in Fig. 5. As the increasing of ZnO content, the dielectric constant increases firstly and then decreases. When ZnO content change from 0.5 wt% to 20 wt%, the dielectric constant decreases from the maximum value of 1935 to the minimum value of 818. The dielectric constant is mainly dependent on A or B ionic radius and crystal cell size [10]. When ZnO content is less than 2 wt%, Zn^{2+} will substitute Ti^{4+} to increase Ti–O octahedral volume, which enlarges anharmonic vibration space of oxide ion, resulting in the increase of dielectric constant of BMAZ ceramics. When ZnO content is more than 2 wt%, excess ZnO (>2 wt%) will react with Al_2O_3 to generate $ZnAl_2O_4$ spinel phase with lower dielectric constant. Thus more

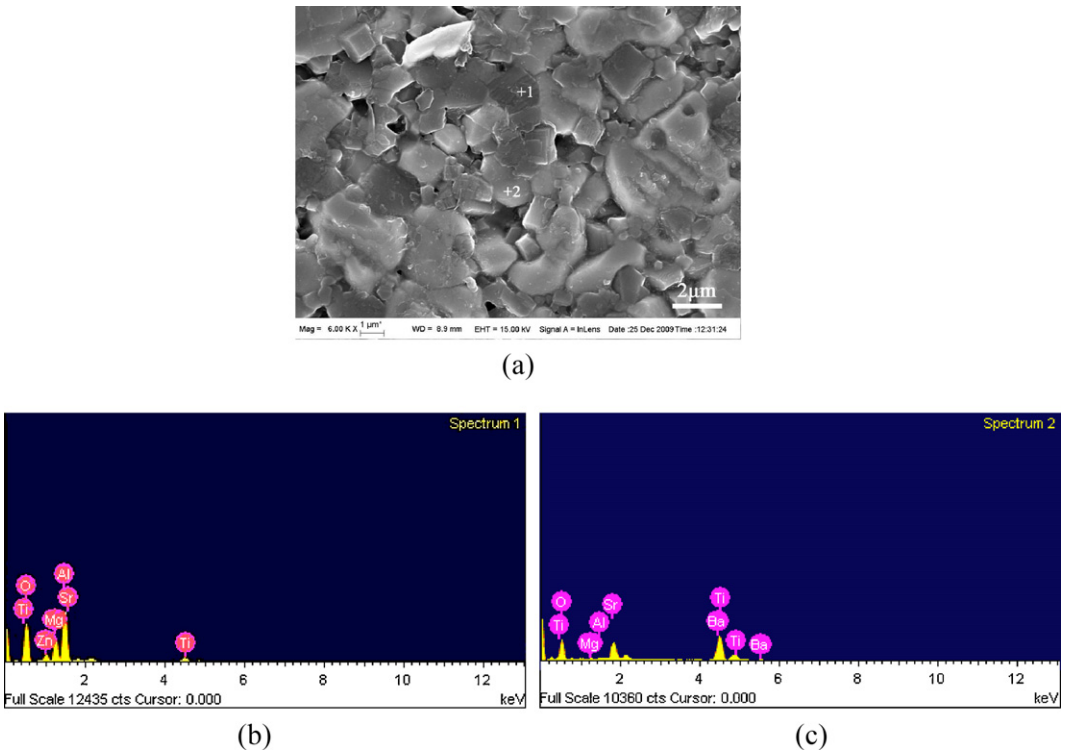

Fig. 4. SEM image and EDS patterns for BMAZ-4# sample: (a) SEM image for BMAZ-4# sample, (b) EDS patterns for spot 1, (c) EDS patterns for spot 2.

Ba^{2+} and Sr^{2+} with larger ionic radius will enter into $ZnAl_2O_4$ and $MgAl_2O_4$ to substitute Zn^{2+} and Mg^{2+}, inducing to the decrease of lattice constant and crystal cell volume of BMAZ. It will restrict the speed and space of oxide ion transport to lead the decrease of dielectric constant of BMAZ ceramics.

The dielectric loss reduces rapidly with ZnO increasing. The dielectric loss is related with density, grain size, porosity and defects [11]. With increasing of ZnO content, the grains grow larger and larger, resulting in the decrease of the amount of grain boundary. The dissipative energy of ions decreases when ions transfer through the grain boundary, so the dielectric loss is reduced. On the other hand, when Zn^{2+} content exceeds solid solubility limit in the BST, excess Zn^{2+} will occupy the BST grains boundary to reduce the vacancy defect concentration, which results in the decrease in the dielectric loss of BST.

Temperature dependences of the dielectric constant and dielectric loss of BMAZ ceramics measured in the range of 1–100 kHz, are displayed in Fig. 6. The maximum of the relative dielectric constant and dielectric loss is depressed with the increasing of measurement frequency. This indicates that an evident frequency dispersion feature which has been observed in most of the ferroelectric ceramics and thin films [20]. Table 3 shows the dielectric properties of BMAZ1–8# ceramics. Combining Fig. 6 and Table 3, it can be seen that the Curie temperature (T_c) of BMAZ ceramic samples is gradually shifted from 9.5 °C for 0.5 wt% ZnO to −18.4 °C for 20 wt% ZnO. It can be interpreted that the substitution of Ba^{2+} for Zn^{2+} in the $ZnAl_2O_4$ lattice is driven by the combination of size and electronegativity difference between Sr^{2+} and Ba^{2+}, resulting in the decrease in Ba/Sr ratio of BST and thereby the decrease in T_c.

There are obvious loss peaks near the paraelectric–ferroelectric phase transition points. This means that the loss increases when BMAZ ceramics transform from ferroelectric phase to paraelectric phase. At the same time, the loss peaks are depressed obviously as ZnO content increasing, which consists with previous analysis results.

Table 2
EDS data of BMAZ-4# sample for spot 1 and 2, as shown in Fig. 4.

Element	Spot 1/atom%	Spot 2/atom%
O	46.04	46.29
Mg	11.30	0.49
Al	26.06	0.77
Ti	6.08	23.64
Sr	3.02	10.56
Ba	2.25	18.25
Zn	5.25	–
Total	100.00	100.00

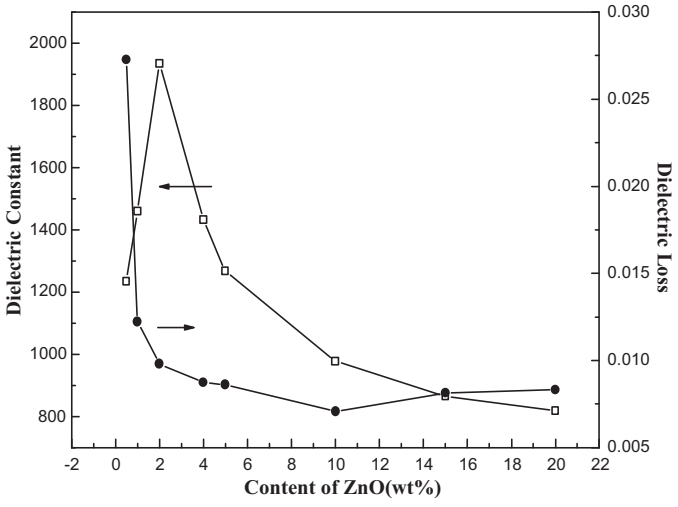

Fig. 5. Dielectric constants and dielectric loss of BMAZ ceramics (10 kHz).

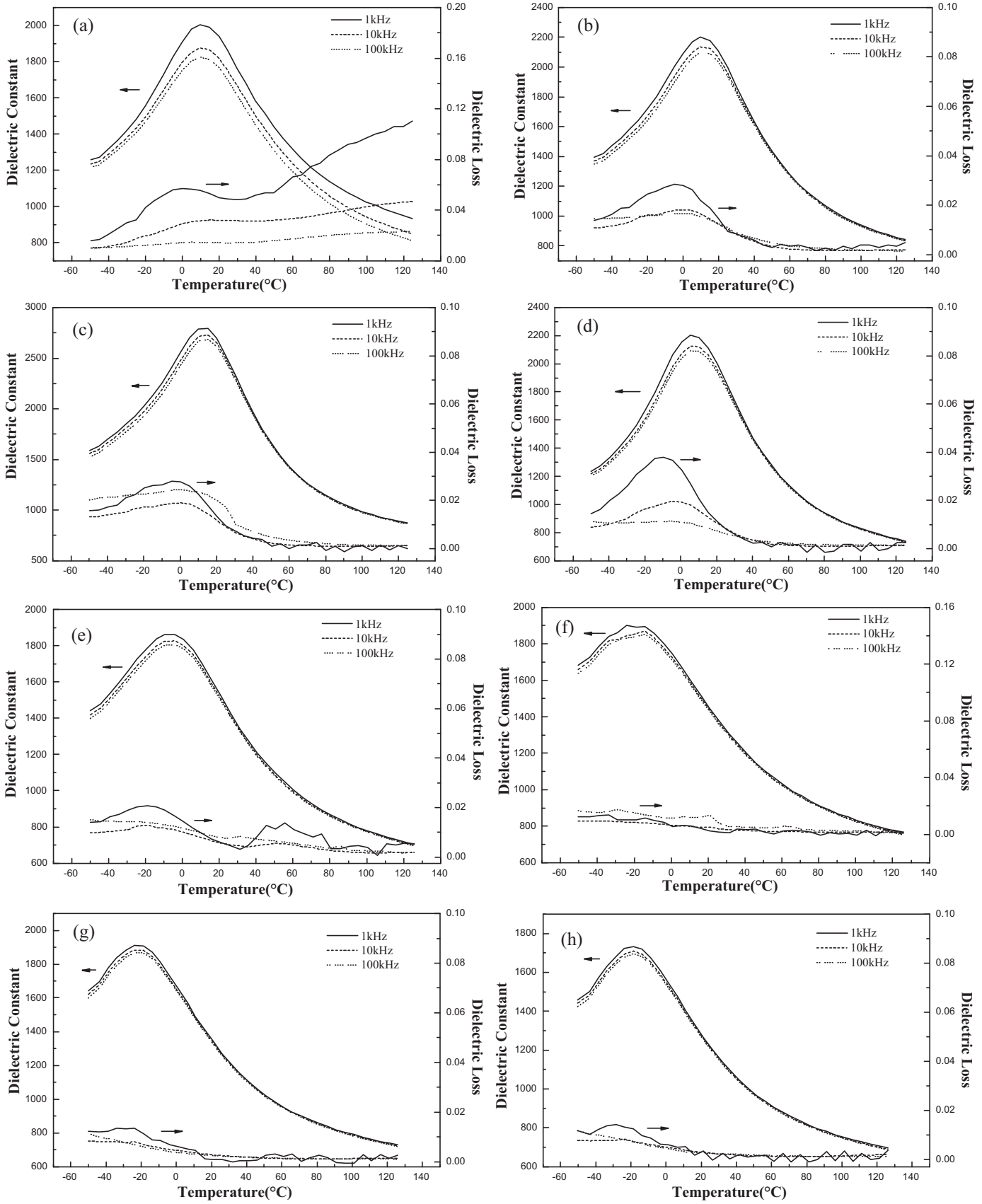

Fig. 6. Temperature denpendence of dielectric constant and dielectric loss of BMAZ ceramics at different frequencies: (a) BMAZ-1#, (b) BMAZ-2#, (c) BMAZ-3#, (d) BMAZ-4#, (e) BMAZ-5#, (f) BMAZ-6#, (g) BMAZ-7#, (h) BMAZ-8#.

Table 3
Dielectric properties of BMAZ1–8# ceramics at 10 kHz.

Composition	T_c (°C)	ε_{max} (T_c)	ε_r (25 °C)	tan δ (25 °C)	Tunability (1.0 kV/mm)
BMAZ-1#	9.5	2018	1235	0.0268	23.4%
BMAZ-2#	10.2	2246	1459	0.0122	27.4%
BMAZ-3#	15.3	2726	1935	0.0095	26.9%
BMAZ-4#	4.6	2234	1432	0.0087	19.3%
BMAZ-5#	−4.3	2272	1268	0.0086	19.0%
BMAZ-6#	−20.3	2070	975	0.0045	11.6%
BMAZ-7#	−23.9	1950	865	0.0075	10.6%
BMAZ-8#	−18.4	1786	818	0.0082	8.9%

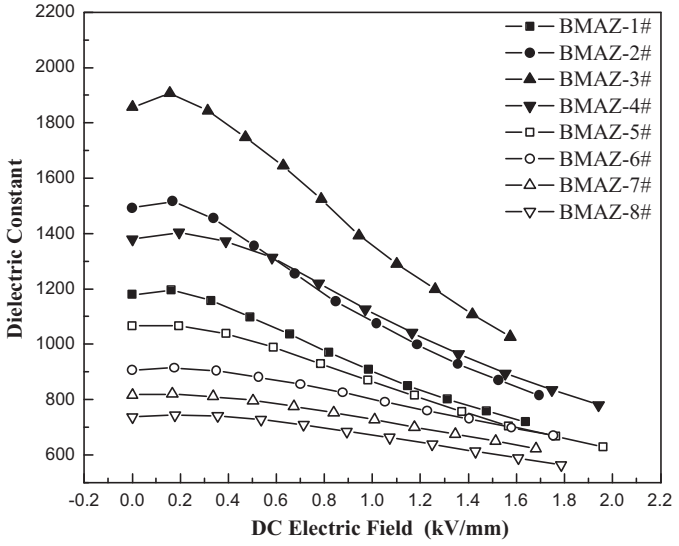

Fig. 7. Electrical dependence of dielectric constant of BMAZ1–8# ceramics (10 kHz).

The electrical dependence of dielectric constant and tunability of BMAZ1–8# ceramics at 10 kHz are shown in Figs. 7 and 8, respectively. As shown in Fig. 7, it is evident that the relative dielectric constant of the samples decreases with increasing the DC biasing field. Many works on the tunability of BST materials tested in different measuring conditions were reported, so it was very difficult to compare them. For examples, $Ba_{0.6}Sr_{0.4}TiO_3/Mg_2SiO_4/MgO$ composites have tunability of 10.5% under electric field of 2.0 kV/mm [21]. The tunability of $Ba_{0.6}Sr_{0.4}TiO_3$ (Mn)/MgO come up to

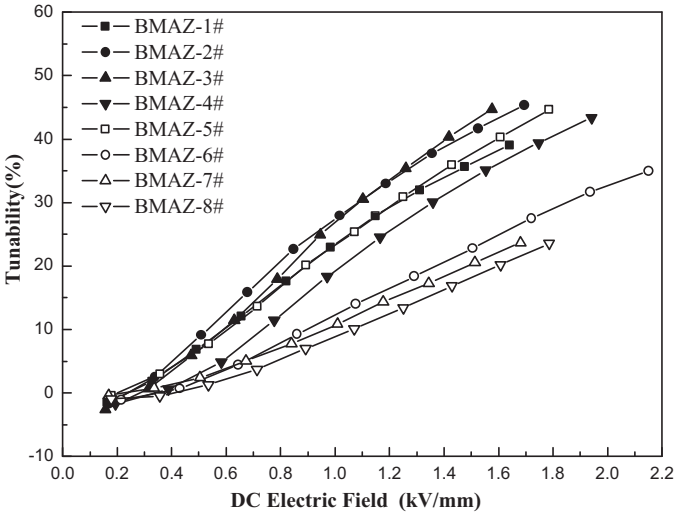

Fig. 8. Electrical dependence of tunability of BMAZ1–8# ceramics (10 kHz).

Table 4
The values of T and T_0 in various ferroelectric materials.

Materials	T (%)	E (kV/mm)	T_0 (mm/kV)	References
$Ba_{0.6}Sr_{0.4}TiO_3/Mg_2SiO_4/MgO$	10.5	2.0	0.053	[21]
$Ba_{0.6}Sr_{0.4}TiO_3$(Mn)/MgO	27.3	8.0	0.034	[22]
$Ba_{0.6}Sr_{0.4}TiO_3$/MgO(3D)	50.0	2.0	0.250	[23]
$Ba_{0.6}Sr_{0.4}TiO_3/Mg_{0.7}Zn_{0.3}TiO_3$	33.5	3.0	0.112	[24]
$Ba_{0.6}Sr_{0.4}TiO_3/Mg_2TiO_4$	38.5	2.0	0.193	[25]
$Ba_{0.6}Sr_{0.4}TiO_3/MgAl_2O_4$	23.6	1.0	0.236	[26]
$Ba_{0.6}Sr_{0.4}TiO_3/MgO/Al_2O_3/ZnO$	27.4	1.0	0.274	–

27.3% under electric field of 8.0 kV/mm dc electric field [22]. The 3D $Ba_{0.6}Sr_{0.4}TiO_3$/MgO composites sintered using SPS have tunability of 50% under electric field of 2.0 kV/mm [23]. The tunability of $Ba_{0.6}Sr_{0.4}TiO_3/Mg_{0.7}Zn_{0.3}TiO_3$ composite ceramics is 33.5% under 3.0 kV/mm biasing at room temperature [24]. $Ba_{0.6}Sr_{0.4}TiO_3$/30wt%Mg_2TiO_4 composite ceramics have tunability of 38.5% under electric field of 2.0 kV/mm at 10 kHz and 20 °C [25].

The tunability of BST-based ferroelectric materials is enhanced with increasing of applied electric field, as shown in Fig. 8. It is necessary to determine same conditions to compare the tunability of different BST-based materials, such as the testing frequency and applied electric field. Therefore the comparison criterion for the tunable ceramics is proposed. We define T_0 as the tunability under unit applied electric bias, shown as the following equation:

$$T_0 = \frac{T}{E} \tag{6}$$

where T is the tunability under a specific applied electric bias; T_0 is the slope of tunability curves (Fig. 8); E is a specific applied electric bias ($E \geq 0.5$ kV/mm). Fig. 8 shows that the tunability changes as linear increase when electric bias exceeds 0.5 kV/mm. That means Eq. (6) is applicable when electric bias exceeds a specific threshold voltage. The tunability of BST-based materials is correlative with T_0 value. The larger T_0 value is, the higher the tunability of BST-based material is. In this paper, the comparison criterion condition for tunability of BST-based material is $E = 1.0$ kV/mm. In our previous study [26], the tunability under 1.0 kV/mm biasing was 23.6% for $Ba_{0.6}Sr_{0.4}TiO_3/MgAl_2O_4$ composite ceramics, which means T_0 is 0.236 mm/kV. For the 1.0 wt% ZnO addition, the dielectric constant is cut down from 1492 under zero electric field to 1083 under 1.0 kV/mm biasing, so the tunability is 27.4% according to Eq. (1). The T_0 value of $Ba_{0.6}Sr_{0.4}TiO_3/MgO/Al_2O_3/ZnO$ ceramics is 0.274 mm/kV. In order to compare the tunability of various BST-based ferroelectric materials, the T_0 values are calculated according to Eq. (6), list in Table 4. The tunability of $Ba_{0.6}Sr_{0.4}TiO_3/MgO/Al_2O_3/ZnO$ ceramics is obviously higher than that of other ferroelectric materials in previous reports.

It is well-known that the change of dielectric constant under applied electric field is associated with the anharmonic interactions of Ti^{4+} ions for paraelectric BST-based material system [27]. From Table 3 results, it can be seen the tunability increases first and then decreases. This can be explained that Ti^{4+} is substituted by Zn^{2+} with larger radius when ZnO is doped in the first instance, which induces the Ti–O octahedron volume to enlarge. Thus, Ti^{4+} will move in larger area under a bias field, resulting in the increase of tunability. As ZnO content further increasing, excess ZnO will react with Al_2O_3 to produce a great deal of non-ferroelectric phase $ZnAl_2O_4$, while ferroelectric phase BST decreases at the same time.

4. Conclusions

The effect of co-doping ZnO, Al_2O_3 and MgO on the microstructures and dielectric properties of $Ba_{0.6}Sr_{0.4}TiO_3$ ceramics was investigated. Two crystalline phases, a cubic perovskite phase

$Ba_{0.6}Sr_{0.4}TiO_3$ and a face-centered-cubic spinel phase $Mg(Zn)Al_2O_4$ were observed. With the increase of ZnO, the paraelectric-ferroelectric phase transition points of BMAZ ceramics shift to the lower temperatures, and the maximum of dielectric constant increased first and then decreased. A comparison criterion for the BST-based tunable ceramics was proposed. A higher tunability which amounts to 27.4% under 1.0 kV/mm biasing was obtained for BMAZ ceramics doped with 1.0 wt% ZnO.

Acknowledgments

This work was supported by Aviation Science Foundation of China (2009ZF53061), Basic Research Foundation of Northwestern Polytechnical University (G9KY101902), and the Doctorate Foundation of Northwestern Polytechnical University (cx201010).

References

[1] J.W. Zhai, H. Chen, C.C. Chou, J. Alloys Compd. 509 (2011) 6113–6116.
[2] H.T. Jiang, J.W. Zhai, X.J. Chou, et al., Mater. Res. Bull. 44 (2009) 566–570.
[3] F. Ponchel, D. Rémiens, J. Midy, et al., J. Am. Ceram. Soc. 94 (2011) 1661–1663.
[4] R. Reshmi, A.S. Asha, P.S. Krishnaprasad, et al., J. Alloys Compd. 509 (2011) 6561–6566.
[5] J.J. Zhang, J.W. Zhai, X.J. Chou, Acta Mater. 57 (2009) 4491–4499.
[6] T. Wang, F. Gao, G.X. Hu, et al., J. Alloys Compd. 504 (2010) 362–366.
[7] D. Zhang, T.W. Button, V.O. Sherman, J. Eur. Ceram. Soc. 30 (2010) 407–412.
[8] M.W. Zhang, J.W. Zhai, B. Shen, et al., J. Am. Ceram. Soc. 94 (2011) 3883–3888.
[9] W.Y. Park, C.S. Hwang, J.D. Baniecki, et al., Appl. Phys. Lett. 92 (2008) 102902.
[10] L.N. Gao, J.W. Zhai, X. Yao, Appl. Surf. Sci. 255 (2009) 4521–4525.
[11] M. Adamczyk, Z. Ujma, L. Szymczak, J. Eur. Ceram. Soc. 26 (2006) 331–336.
[12] Y.Y. Zhang, G.S. Wang, Y. Chen, et al., J. Am. Ceram. Soc. 92 (2009) 2759–2761.
[13] G.X. Hu, F. Gao, X. Cao, et al., Mater. Sci. Forum 687 (2011) 327–332.
[14] Y.C. Lee, T.K. Lee, J.H. Jan, J. Eur. Ceram. Soc. 31 (2011) 3145–3152.
[15] F. Rubio-Marcos, J.J. Romero, M.G. Navarro-Rojero, et al., J. Eur. Ceram. Soc. 29 (2009) 3045–3052.
[16] G.X. Dong, S.W. Ma, J. Du, Ceram. Int. 35 (2009) 2069–2075.
[17] F. Gao, R.Z. Hong, J.J. Liu, et al., J. Eur. Ceram. Soc. 29 (2009) 1687–1693.
[18] E.M. Levin, C.R. Robbins, Phase Diagrams for Ceramists, The American Ceramic Society Inc., Columbus, 1975, Fig. 4331.
[19] E.M. Levin, C.R. Robbins, Phase Diagrams for Ceramists, The American Ceramic Society Inc., Columbus, 1969, Fig. 299.
[20] F. Gao, L.L. Liu, B. Xu, et al., J. Alloys Compd. 509 (2011) 6049–6055.
[21] Y. He, Y. Xu, T. Liu, et al., IEEE Trans. Ultrason. Ferroelectr. Freq. Control 57 (2010) 1505–1512.
[22] J.D. Cui, G.X. Dong, Z.M. Yang, et al., J. Alloys Compd. 490 (2010) 353–357.
[23] U.C. Chung, C. Elissalde, M. Maglione, Appl. Phys. Lett. 92 (2008) 042902.
[24] J.J. Zhang, J.W. Zhai, X.J. Chou, et al., Solid State Commun. 147 (2008) 392–396.
[25] P. Liu, J.L. Ma, L. Meng, et al., Mater. Chem. Phys. 114 (2009) 624–628.
[26] G.X. Hu, F. Gao, L.L. Liu, et al., Ceram. Int. 37 (2011) 1321–1326.
[27] K.M. Johnson, J. Appl. Phys. 33 (1962) 2826–2831.